ANUBIS Single Tracking Station RPC Geometry Investigation

Blind grade number: 8274Q
University of Cambridge, UK
Supervisor: Jon Burr, Oleg Brandt

May 16, 2022

Statement: Except where specific reference is made to the work of others, this work is original and has not been already submitted either wholly or in part to satisfy any degree requirement at this or any other university.

Code: https://drive.google.com/file/d/1_RKwNnmXxig5v7AywAD3vMRidRkPUdN1/view?usp=sharing

Abstract

The current Standard Model has been tested and verified to be accurate in many studies. However, there are still many questions that remain unanswered, these include the existence of Dark Matter, baryon asymmetry and neutrino masses. As a result, Beyond Standard Model theories have been introduced, in which many of those models predict Long-Lived Particles (LLP). ANUBIS is a newly proposed detector that will enhance the sensitivity of LLP detection in the scalar Higgs Portal model. Compared with the existing ATLAS analysis[4], ANUBIS is expected to produce an LLP sensitivity that is better by more than two orders of magnitude at decay lengths 10-100 m. This project aims at using Monte Carlo samples from the gluon-gluon fusion (ggF) channel to examine the sensitivity of vertex reconstruction in one ANUBIS Tracking Station (TS) with the parallel and offset arranged RPC readout strips. Simulations show that for a TS located at a distance $1 - 10m$ away from the LLP decay point and with a typical strip pitch 2.5cm, the offset arrangement is producing a better reconstructed vertex in 70% of the times. For a TS located at a distance 1m away but with a strip pitch varying from 1.0cm to 3.5cm, the offset arranged strips is better in most of the times, but the advantage of using the offset arrangement is getting smaller as we use smaller strips.

Contents

1 Introduction

The Standard Model (SM) in Particle Physics is one of the most well-tested models. It has been verified to be consistent with experimental observations to a high order of precision. However, the SM does not tell the full story, there are still many other phenomena such as the existence of Dark Matter (DM), neutrino masses and baryon asymmetry, which cannot be explained. As a consequence, theorists came up with Beyond Standard Model (BSM) theories to solve the puzzle, and many of them predict particles with long lifetimes, which are also called Long-Lived Particles (LLP).

Physicists have performed extensive analyses on LLP signatures using measurements from the ATLAS [4, 6, 5], CMS [18, 3] and LHCb [7] detectors to examine their properties. To improve further the LLP sensitivity, several new experiments have been designed. Examples of such an experiment include FASER [9, 13], MATHUSLA [16] and ANUBIS [10] which are proposed to be installed next to either ATLAS or CMS; and the CODEX-b [14] detector is proposed to be installed next to LHC-b.

This project will be focusing on the neutral LLP signatures predicted by the scalar Higgs portal model in the proposed ANUBIS detector. Monte Carlo samples generated from the gluon-gluon fusion (ggF) channel at an LLP mass of 10 GeV are used to obtain the distribution of LLPs and their charged final states. In the simulation, LLPs are rotated so it appears to be coming from the Large Hadron Collider (LHC) interaction point, and the same rotation matrix is applied to their decayed particles.

Six layers of Resistive Plate Chamber (RPC) detectors that extend infinitely in the plane perpendicular to the incoming LLP are simulated in the way that they have the same spacing as proposed in the ProANUBIS project. ProANUBIS is a Tracking Station (TS) module sized $1 \times 1 \times 1m^3$ to be installed around ATLAS and make measurements during LHC Run 3 to study the performance of ANUBIS. The use of detectors that are infinitely large is only an approximation, as the actual TS has an area limited by the cross-sectional area of the shaft.

The charged LLP final particles will create a signal when it hits the simulated detector plane. Final state tracks and their vertices are reconstructed using these hit points. The distribution of displacement between the true vertex and the reconstructed vertex for different LLP geometries is compared to see which is giving a better vertex reconstruction resolution overall. Variables such as RPC perpendicular distance to decay point (L), detector strip pitch (p) and the projected hit position of incoming LLP is changed to test the reconstruction behaviour under different environments. An illustration of L and p is shown in Figure 1, while the meaning of the projected hit position of the incoming LLP is explained in section 5.1.

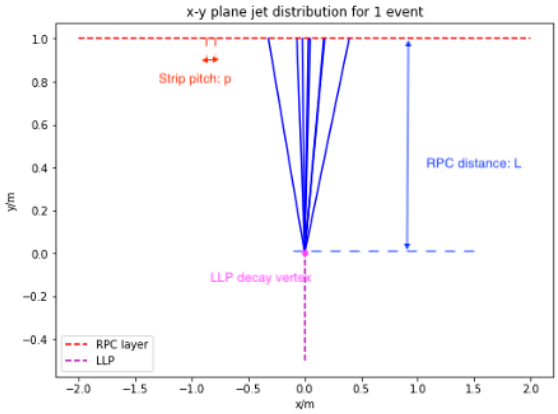

Figure 1: A simulated LLP decay event with first RPC layer placed at distance L, strip pitch p. The blue lines represent the decayed charged final states of LLP, the red dashed line represent RPC detectors and the pink dashed line represent the incoming LLP.

In this report, the theory of the scalar Higgs Portal model predicted LLP and its detector signatures are described in section 2; the motivations of ANUBIS, its proposed geometry and the physics behind RPC detectors will be discussed in section 3; details of detector simulation and vertex reconstruction method used in this project is explained in section 4, and section 5 contains a summary of the analysis of different RPC geometries experimented in this project; finally, a conclusion is situated at the end of this report.

2 Theoretical Background

As mentioned in section 1, there is the need for BSM theories to explain the addressed open questions. Many of the BSM models predict the existence of LLPs, examples of such a model include Supersymmetry (SUSY), Neutral Naturalness, interactions in association with DM production and portal interactions with the Hidden Sector, a detailed discussion about theoretical models can be found in reference [12]. There already exist several analyses to measure the LLPs predicted by their relevant models. The proposed LLP detectors such as MATHUSLA and ANUBIS make use of the Scalar Higgs Portal model, and this is the model that is most relevant to this project.

2.1 Scalar Higgs Portal Model

Hidden Sector Portal Models refer to Hidden Sector interactions with SM particles via a mediating field which we call a 'Portal'. Common portals include scalar fields (s), pseudoscalar fields (a), vector fields and neutrino fields. The Scalar Higgs portal model extends from SM by having an additional scalar field s which interacts with SM Higgs Boson h. Its Lagrangian expression can be written as [15]:

$$\mathcal{L} \supset -\frac{\epsilon}{2} S^2 |H|^2 + \frac{\mu_S}{2} S^2 - \frac{\lambda_S}{4} S^4 + \mu_H^2 |H|^2 - \lambda_H |H|^4 \tag{1}$$

For which S and H correspond to the Scalar singlet and the SM Higgs doublet respectively. The Feynman diagram of the leading order di-scalar production from a Higgs boson($h \to ss$) can be found in Figure 2, where empty circles represent point interactions. This is one of the main interaction processes being considered at the ANUBIS detector, a predicted sensitivity to such a process will be summarised

in section 3.1.

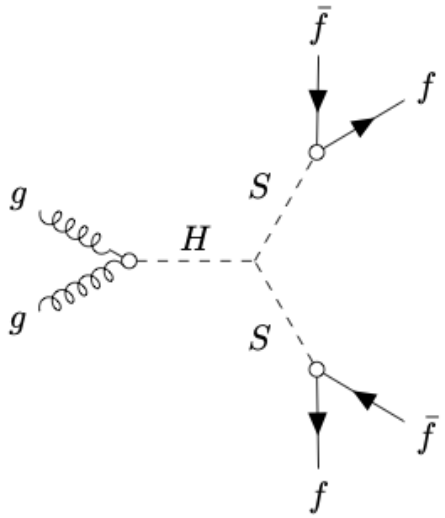

Figure 2: A general Feynmann diagram showing the pp interaction producing a Higgs coupling to two scalar particles, which then decay into Fermions as their final states.

2.2 LLP Signatures

The scalar Higgs Portal model deals with neutral LLPs, which will not produce any direct signals inside the detector. However, these LLPs can decay into charged final states which will leave tracks inside the detector. Because the charged final states originate from the decay point of LLP rather than the LHC Interaction Point (IP), they will appear as displaced tracks. A displaced vertex is when multiple LLP daughter tracks join at a common origin. Hence, a neutral LLP can be identified using this feature and its decay length can be calculated by measuring the location of the displaced vertex. This project is focusing on the simulation of charged final state signals on RPC detectors and the investigation of vertex reconstruction efficiency when different detector geometries are implemented. Other indirect or direct detection methods of the LLP can be found in [15].

3 ANUBIS Detector

3.1 Motivation

Previous LHC searches for LLP production in the Higgs portal model have been performed in ATLAS [4, 6, 5], CMS [18, 3] and LHCb [7] to examine the $h \to ss$ process. It is possible to compare the sensitivity measured at ATLAS, CMS and LHCb with the projected ANUBIS sensitivity. Figure 3 demonstrates the sensitivity simulated for ANUBIS [10], CODEX-b [14], MATHUSLA [16] and the sensitivity measured at ATLAS in the plane of the $h \to ss$ Branching Ratio (BR) and the scalar particle lifetime (τ_s), where s is expected to be the LLP. The Long-Lived Particles are less likely to decay to subsequent states at a short distance away (i.e. at small $c\tau_s$) from the IP as they are expected to be long-lived; at larger distances from the IP, the detector sensitivity drops and the combined effect of these two factors results in the

overall bell-shaped curves in the $BR - c\tau_s$ plane.

In Figure 3, two projections of ANUBIS are shown with the 4-events being the optimal case for detection of new physics by assuming a very small background; 50-events being the conservative case with a standard background estimate. The shaded region for the ANUBIS curves represents the difference between having one tracking station or all four equally spaced tracking stations inside the PX14 shaft. The simulated ANUBIS sensitivity has a $BR(h \to ss)$ lower bound in the scale of $\sim 10^{-5}$ between regions 1m$< c\tau_s <$ 100, and it is a large improvement based on the previous ATLAS measurement (shaded in blue) which has a $BR(h \to ss)$ lower bound in the scale of $\sim 10^{-3}$ between regions 1m$< c\tau_s <$ 100m. In the paper [10], the ANUBIS sensitivity is estimated by simulating the Higgs scalar portal model ($h \to ss$) using `MADGRAPH5` [8], and the decays are only counted when they penetrate at least one of the TSs.

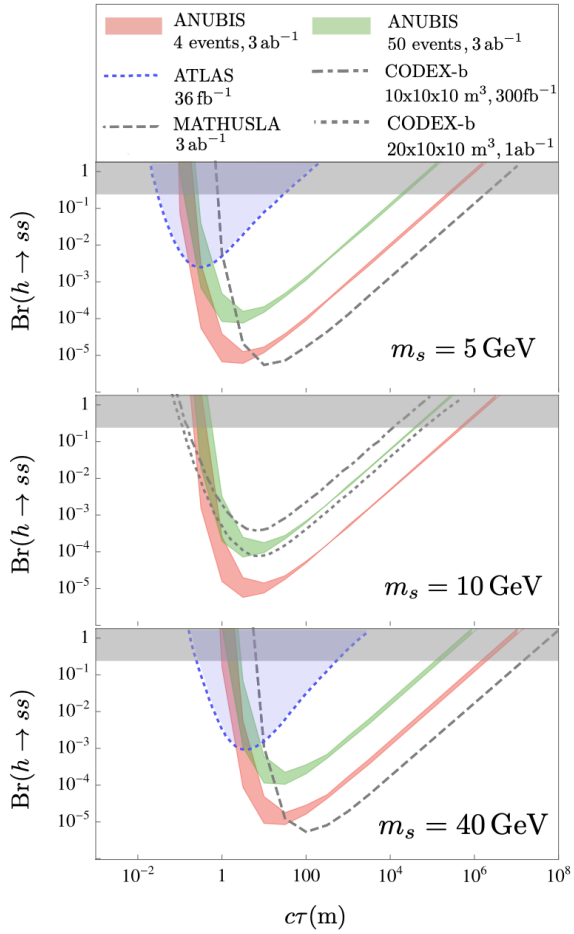

Figure 3: The simulated ANUBIS $h \to ss$ sensitivity compared with previous ATLAS [4] sensitivity and expected MATHUSLA [16] and CODEX-b [14] sensitivity. Cases of LLP masses $m_s = 5, 10, 40$ GeV are shown in top, middle, and bottom respectively. (Graph from [10])

3.2 ANUBIS Layout

The proposed ANUBIS detector contains four Tracking Station (TS)s spaced out equally at a distance of 18.5m inside the ATLAS PX14 shaft, and it will be aiming for the off-axis interactions. Each TS is rounded and concentric with the shaft to maximise acceptance. However, the TS planes are not perfect circles due to the pipework in the shaft as shown in Figure 4. Each of the TS is made of six layers of RPC, the current proposed structure for ProANUBIS is the triplet-singlet-doublet design to maximise track identification efficiency, this is shown in Figure 5.

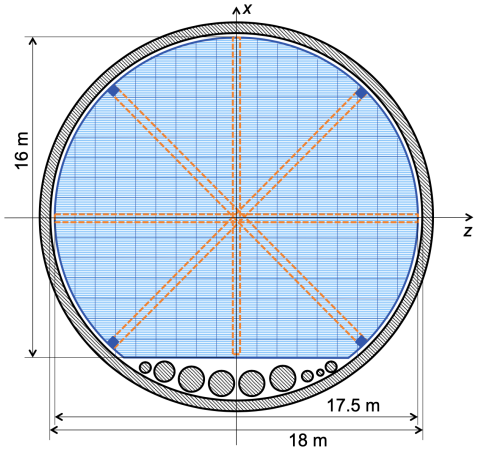

Figure 4: One of the ANUBIS TS viewed from above - in the x-z plane. The TS is shaded in blue, the shaft wall and pipework are shaded in black and the orange lines represent the TS supporting structure. (Graphs from [10].)

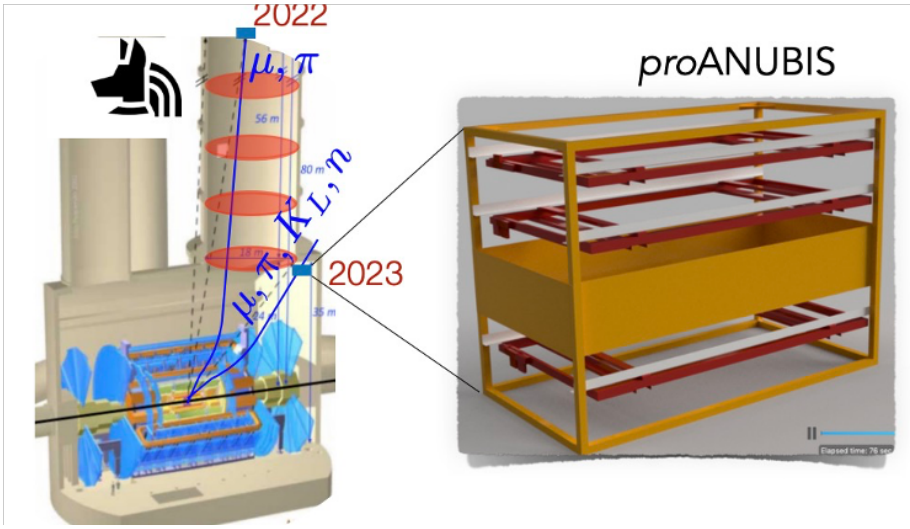

Figure 5: The position of the TS inside the shaft and the layout of RPC detectors in ProANUBIS. (Graph from the ANUBIS group.)

3.3 Resistive Plate Chamber (RPC)

The ANUBIS detector will be using the BIS78 RPC units as described in the ATLAS Phase-II upgrade [2]. The schematic diagram of an RPC singlet can be found in Figure 6. The key components of such a detector include the orthogonal readout strips situating at the top and bottom to together give a 2-dimensional reading; and the gas gap sandwiched between to provide a space for particle ionisation. When a charged particle travels through a unit of RPC, it ionises the gas particles inside the 1mm gap. These ionised particles will continue travelling and ionise more particles inside the gap to eventually create a charge avalanche. The positive and negatively charged ions created will get attracted to the corresponding plates and hence creating a signal on the readout strip. This study will simulate the signals obtained from the readout strips to reconstruct the particle tracks, and the actual thickness of an RPC layer is ignored.

A triplet RPC is achieved by boxing three singlets together. According to studies, RPC time resolution scales with the thickness of gas gaps due to the change in ionisation density [11], therefore the ungraded Phase-II ATLAS RPC singlet is constructed with $\sim$ 1mm gap. Hence improving the time resolution from $\sim$ 1ns to $\sim$ 0.4ns [17]. BIS78 RPC is built to be compatible with HL-LHC [1], therefore by using this, ANUBIS should also be compatible with HL-LHC.

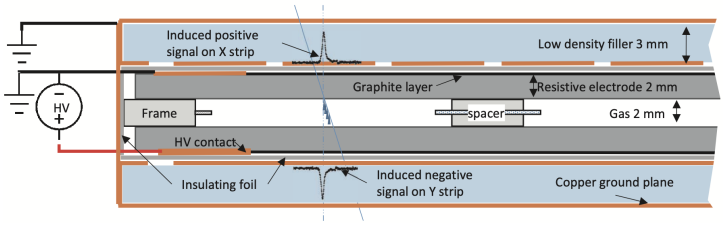

Figure 6: A schematic diagram showing the typical layout of a singlet RPC layer being used in the present ATLAS.(Graph from [2])

4 Detector Simulation

Simulation of particle detection inside one ANUBIS tracking station can be broken down into three main stages. The first stage is to select the neutral LLPs and their daughter particles from the Monte Carlo generated samples to obtain their travelling directions. Then each LLP together with its daughter particles will be rotated so that the LLPs appear to be coming from the LHC interaction point and will be travelling perpendicular to the detector planes. The second stage is to simulate six infinite layers of RPC readout strips, and record a track hit on the strip whenever a particle track goes through it. Then finally reconstruct the tracks and vertices using the track hits on the detector planes to see how well the reconstructed vertices are when different geometries of RPC planes are implemented.

4.1 Event Selection and Track Rotation

The Monte Carlo Generated samples used in this study is the from the ggF channel whose Feynman diagram is illustrated in Figure 7. In order to select the relevant final state particles, each particle in the dataset is assessed with its particle ID and mother particle ID. A particle is selected if it is a decay product of b or $\bar{b}$ and with the condition that $b\bar{b}$ is coming from an LLP (S in the Feynman diagram). Then it must also pass the filter condition to ensure it is charged and is a final state where the term final state refers to particles that are stable and do not decay any further. These selected final states are matched with their parent LLPs, and their angular coordinates ϕ and η are extracted to obtain their

travelling directions. η stands for pseudorapidity and it is converted into normal spherical angle θ using Equation 2

$$\theta = 2\tan^{-1}(e^{-\eta}) \tag{2}$$

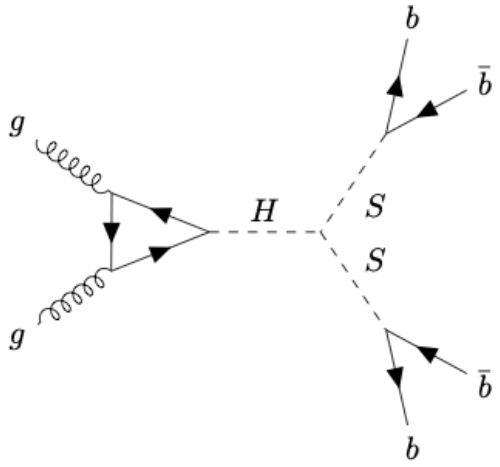

Figure 7: Feynman Diagram of gluon-gluon fusion process in the Scalar Higgs Portal Model

Defining one event as one LLP decaying into its daughter particles. For each selected event, the LLP is rotated so it appears to be coming from the LHC interaction point and is travelling perpendicularly to the detector planes, and then the same rotation matrices are applied to its daughter particles so that the relative angular distributions of the final states remain unchanged. Throughout this process, the ATLAS right-handed coordinate system has been used, where x is pointing towards the centre of the LHC ring, y is the vertical direction, and z is along the beamline. The rotation process can then be summarised in Equation 3.

$$\mathbf{M_1} = \begin{pmatrix} \cos\phi_S & -\sin\phi_S & 0 \\ \sin\phi_S & \cos\phi_S & 0 \\ 0 & 0 & 1 \end{pmatrix}$$

$$\mathbf{M_2} = \begin{pmatrix} 1 & 0 & 0 \\ 0 & \cos\theta_S & \sin\theta_S \\ 0 & \sin\theta_S & \cos\theta_S \end{pmatrix} \tag{3}$$

$$\vec{r'} = \mathbf{M_2}\mathbf{M_1}\vec{r}$$

Where ϕ_S and θ_S are the spherical coordinates of the LLP. Matrix $\mathbf{M_1}$ represents a counter-clockwise rotation with respect to the z-axis by an angle of $\frac{\pi}{2} - \phi_S$ so that the incoming LLP lies in the z-y plane. $\mathbf{M_2}$ is a clockwise rotation around the x-axis by an angle of $\frac{\pi}{2} - \theta_S$, so that the incoming LLP is travelling along the positive y-axis. A visualisation of such a rotation for one event can be seen in Figure 8

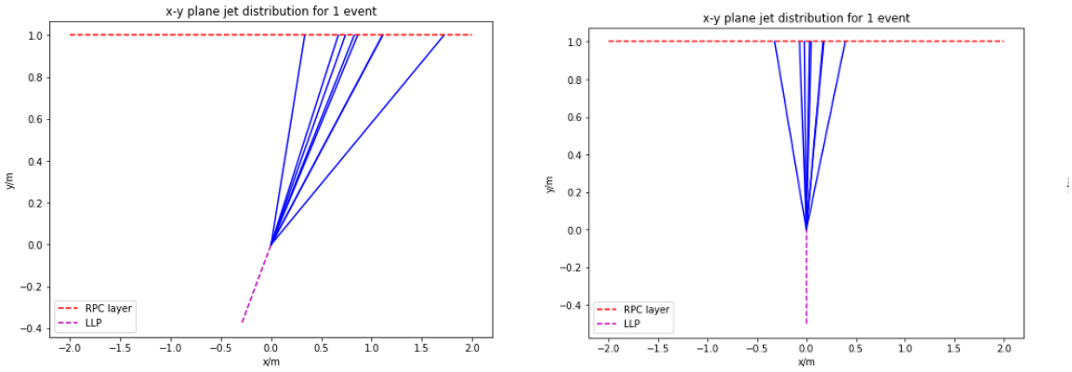

Figure 8: The LLP is the pink dashed line, its charged final states are shown in solid blue lines, and the red dashed lines correspond to RPC detector planes. Left shows the directions of the LLP and its daughter particles before rotation. Right shows the result after applying the rotation matrices. The decay position is intentionally kept at (0, 0, 0) to make later analysis easier.

4.2 Detection Simulation

As discussed in Section 3, the six layers of RPC detectors have the triplet-singlet-doublet layout, and the current proposed relative positions of these layers are shown in Table 1. Where the reference layer is taken to be the singlet layer in the middle (Layer 4).

Layer	1	2	3	4	5	6
Height/m	-0.50	-0.49	-0.48	0.00	0.49	0.50

Table 1: Height of RPC layers in a single tracking station

Each detector strip was initially set to be 2.5cm wide in the simulation, as a typical strip width would be $2 - 3cm$. The current RPC detectors used have parallel aligned strips, where layers of detector strips lie directly above each other, and this will be one of the simulated geometries in this study. In addition, another geometry where the closely packed layers are displaced relative to one another has been tested and its result is compared with the parallel arranged strips in later sections. The displacement of the strips relative to each other in closely packed RPC layers Δx is maximised by having $\Delta x = p/3$ for the bottom triplet, where p is the strip pitch; and $\Delta x = p/2$ for the top doublet. Examples of the parallel and off-set arranged RPC layers are illustrated in Figure 9. This graph applies to both the x-y and z-y planes, and this simulation assumes infinite RPC sheets in the x-z plane.

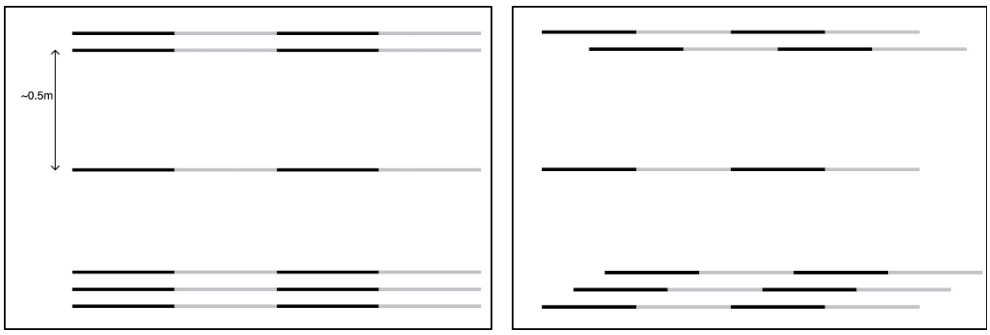

Figure 9: A schematic graph showing the parallel (Left) and off-set (Right) arrangement of RPC readout strips, with the layer separations equal to the values discussed above. All black and grey line segments represent identical RPC readout strips, the colour difference is just to make neighbouring strips distinguishable from each other. This graph is not to scale.

When a particle goes through a tracking station, it will hit one strip on each layer. For this simulated detector, it will not tell the exact location of the hit, but instead, it will consider the location of the strip that got hit and take the hit position to be situated at the strip centre with an error of

$$\sigma = p/\sqrt{12} \tag{4}$$

4.3 Reconstruction

As described in the previous section, for each final state particle, it will leave a hit on each RPC layer i.e. a total of six hit points for each track. These hit points can then be used to reconstruct the final state particle tracks and the LLP decay point.

4.3.1 Method 1 - Independent Track Reconstruction (ITR)

This method fits each track in an event separately and finds the point at which the distance to all reconstructed tracks is minimised. This point is then taken to be the vertex. Each track is fitted using `scipy.optimize.curve_fit()` [19] function to carry out a linear regression analysis. An important assumption made here is that we have prior knowledge of which hit belongs to which track. After all tracks in one event are fitted, we find the vertex by first defining a random point on the plane:

$$\vec{r_p} = (x_p, y_p, z_p) \tag{5}$$

The χ^2 expression can be written as

$$\chi^2 = \sum_i^n |\vec{r_i} - \vec{r_p}|^2 = \sum_i^n \sqrt{(x_i - x_p)^2 + (z_i - z_p)^2} \tag{6}$$

Where $\vec{r_i} = (x_i, y_p, z_i)$ is the position of the hit point created by the i^{th} track on the x-z plane defined by $y = y_p$. There is a total of n tracks in an event.

x_i and z_i can be substituted using the straight-line equation obtained from track linear regression fit.

$$\begin{aligned} x_i &= \frac{y_p - C_{x,i}}{m_{x,i}} \\ z_i &= \frac{y_p - C_{z,i}}{m_{z,i}} \end{aligned} \tag{7}$$

Where $m_{x,i}$, $m_{z,i}$ represents the gradient of i^{th} track in x-y and z-y planes respectively. Similarly, $C_{x,i}$, $C_{z,i}$ are the intercepts for the i^{th} track in x-y and z-y planes respectively. These parameters are obtained from track reconstruction earlier.

Substituting Equation 7 to Equation 6 and minimise χ^2 with respect to $\vec{r_p}$. This minimised point can then taken to be the location of the vertex. The process of track and vertex reconstruction using this method is visualised in Figure 10 for a randomly selected event.

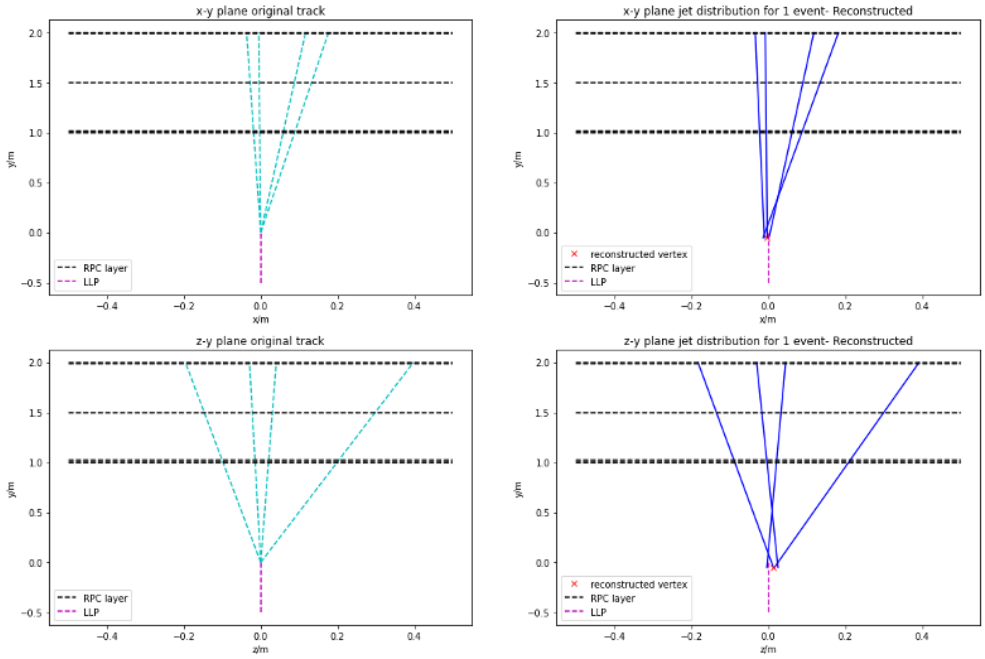

Figure 10: Track and vertex reconstruction for a randomly selected event with parallel RPC strips and first RPC layer placed at 1m away from decay point. Blue lines are final state tracks, the pink line is the LLP track, black dashed lines are RPC detectors, and red crosses in the diagrams on the right are reconstructed vertices. The top left and bottom left diagrams represent the true tracks from the decay of an LLP in x-y and z-y planes respectively. The top right and bottom right diagrams represent the reconstructed final-state tracks from detector hits in x-y and z-y planes respectively.

The distances between reconstructed vertices $\vec{r_p}$ and the true vertex $\vec{r_t}$ can be defined as

$$\begin{aligned} d_R &= |\vec{r_p}| \\ d_{xz} &= \sqrt{x_p^2 + z_p^2} \\ d_y &= |y_p| \end{aligned} \tag{8}$$

As we have set $\vec{r_t} = (0, 0, 0)$. d_R is the 3-D distance, d_{xz} is the distance in x-z plane and d_y is the distance along positive y-direction. A distribution of d_R, d_{xz} and d_y can be obtained by running the first 3000 events as shown in Figure 11.

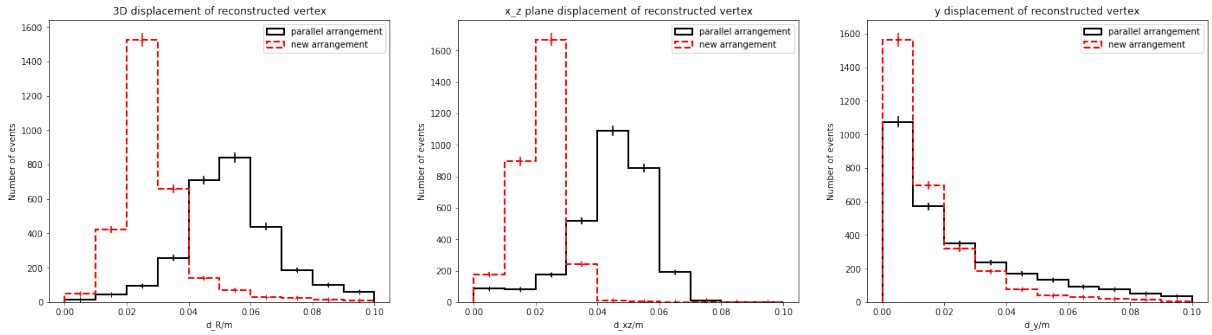

Figure 11: Vertex Reconstruction resolution distribution for 3000 events. Left is the distribution of 3-D displacement between reconstructed vertex and true vertex. The middle is the x-z plane displacement, and the right is the displacement along the y-axis. This is run with $p = 2.5$cm, $L = 1$m.

4.3.2 Method 2 - Constrained Track Reconstruction (CTR)

CTR involves fitting all the tracks in one event at the same time with the constraint that they all converge at one point: the vertex. This is again assuming that we have prior knowledge of which hit belongs to which track, and it additionally assumes all the tracks should cross at one point. Suppose we have the vertex point at:

$$\vec{r_0} = (x_0, y_0, z_0) \tag{9}$$

Then straight line equations in x-y and z-y planes for a track that goes through $\vec{r_0}$ can be written as follows:

$$\begin{aligned} x &= m^{(x)}(y - y_0) + x_0 \\ z &= m^{(z)}(y - y_0) + z_0 \end{aligned} \tag{10}$$

Where $m^{(x)}$ and $m^{(z)}$ are gradient coefficients in the x-y and z-y planes respectively. Assuming no errors in the y-direction and a Gaussian probability distribution in both x and z directions on the strip. The probability distributions can be expressed as:

$$\begin{aligned} P(x_i) &= \frac{1}{\sigma_x\sqrt{2\pi}} e^{-(x_i - \bar{x_i})^2/2\sigma_x^2} \\ P(z_i) &= \frac{1}{\sigma_z\sqrt{2\pi}} e^{-(z_i - \bar{z_i})^2/2\sigma_z^2} \end{aligned} \tag{11}$$

Where here i correspond to the i^{th} RPC layer, $i \in \{1, 2, 3, 4, 5, 6\}$. Here $\bar{x_i}$ and $\bar{z_i}$ are taken to be the mean values i.e. the position of the centre of the strip that got hit by a track on the i^{th} layer.

The likelihood function is given by the product of all the probability distribution functions.

$$L = \prod_i P(x_i)P(z_i) \tag{12}$$

Taking the logs of this likelihood function

$$\ln L = -\frac{1}{2}\sum_i^6 \frac{(x_i - \bar{x_i})^2}{\sigma_x^2} - \frac{1}{2}\sum_i^6 \frac{(z_i - \bar{z_i})^2}{\sigma_z^2} + ... \tag{13}$$

Two terms expressed here can be written as $-\chi^2$ for one track. To maximise likelihood, χ^2 needs to be minimised. Substituting Equation 10, we express χ^2 for a single track to be

$$\chi^2_{OneTrack} = \sum_i^6 \left(\frac{(m^{(x)}(y_i - y_0) + x_0 - \bar{x}_i)^2}{\sigma_x^2} + \frac{(m^{(z)}(y_i - y_0) + z_0 - \bar{z}_i)^2}{\sigma_z^2} \right) \tag{14}$$

Then generalise it to n tracks

$$\chi^2 = \sum_k^n \sum_i^6 \left(\frac{(m_k^{(x)}(y_i - y_0) + x_0 - \bar{x}_{i,k})^2}{\sigma_x^2} + \frac{(m_k^{(z)}(y_i - y_0) + z_0 - \bar{z}_{i,k})^2}{\sigma_z^2} \right) \tag{15}$$

Where $m_k^{(x)}$ is the gradient coefficient in x-y equation for the k^{th} track, $\bar{x}_{i,k}$ is the x coordinate of the mid-point of strip that got hit by the k^{th} track on the i^{th} layer, similar explanations goes for z; y_i is the height of the i^{th} RPC layer; $\sigma_x = \sigma_z = p/\sqrt{12}$ as discussed in Equation 4.

By minimising Equation 15 with respect to $\{m_k^{(x)}, m_k^{(z)}, x_0, y_0, z_0\}$ using `scipy.optimize.minimize()` [19], all of the tracks in one event will be reconstructed simultaneously and will converge at a point. This process is demonstrated in Figure 12. Using the parameter definitions in Equation 8 and run the process

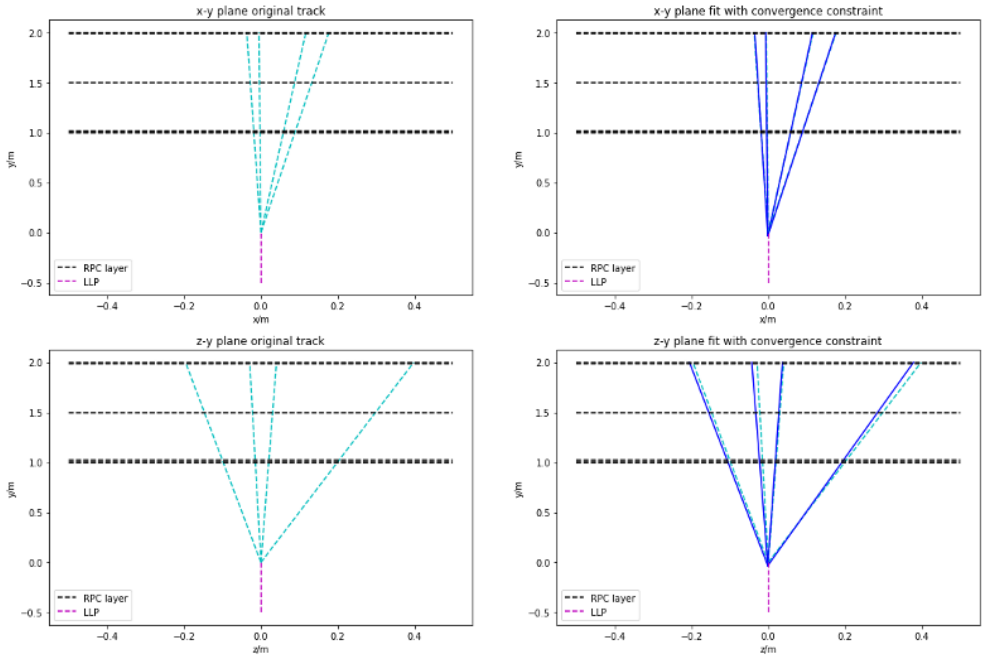

Figure 12: Track and vertex reconstruction for a randomly selected event with parallel RPC strips and first RPC layer placed at 1m away from decay point. Blue lines are final state tracks, the pink line is the LLP track, black dashed lines are RPC detectors, and red crosses in the diagrams on the right are reconstructed vertices. The top left and bottom left diagrams represent the true tracks from the decay of an LLP in x-y and z-y planes respectively. The top right and bottom right diagrams represent the reconstructed final-state tracks from detector hits in x-y and z-y planes respectively.

for the first 3000 events, a distribution of the distances between reconstructed vertices and true vertices can be obtained as shown in Figure 13.

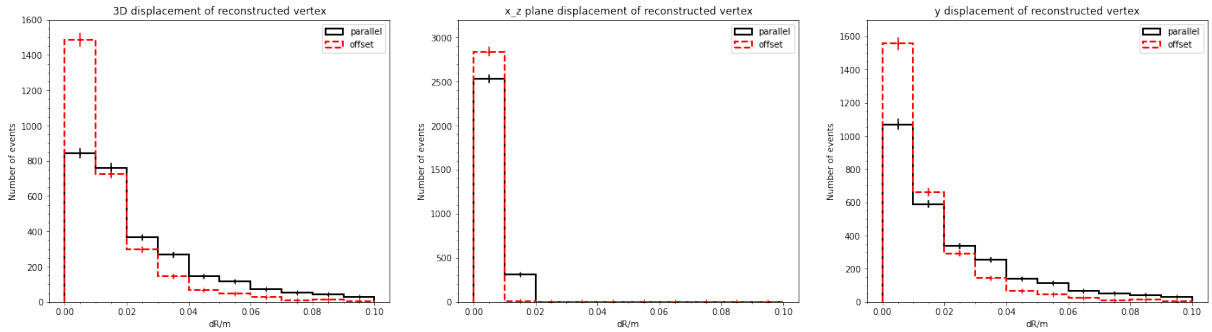

Figure 13: Vertex Reconstruction resolution distribution for 3000 events. Left is the distribution of 3-D displacement between reconstructed vertex and true vertex. The middle is the x-z plane displacement, and the right is the displacement along the y-axis.

4.3.3 Method Comparison

Comparing the distributions shown in Figure 11 and Figure 13, it is clear that the CTR method is providing a better vertex reconstruction than the ITR method as the peaks of the distributions are closer to zero for both parallel and off-set arrangements. Although this means the position of the reconstructed vertex from the CTR method is generally closer to the true vertex position, it makes an additional assumption that all tracks converge to one vertex. Therefore ideally, the ITR method should be used to first identify whether tracks originate from one point, and then those selected tracks will be reconstructed again using CTR to make a more accurate vertex estimation. As this study is focusing on the accuracy of vertex estimation with different RPC geometries, later analysis will be based on the CTR method. From the distributions shown at this point, the offset arrangement is giving a better result for both methods, a more detailed comparison of these two different geometries will be presented in section 5.

5 Results and Discussion

5.1 Projected hit position of the incoming LLP

Using the middle singlet RPC layer as a reference, the incoming LLP can have a projected hit position on the strips. Figure 13 is plotted with the projected track of the incoming LLP hitting exactly at the edge of one of the strips in the middle layer. A schematic diagram of this situation is shown in Figure 14. In the real scenario, the projected incoming LLP track can hit at any point along the strip, hence this hitting position is shifted to see how the distribution of d_R changes.

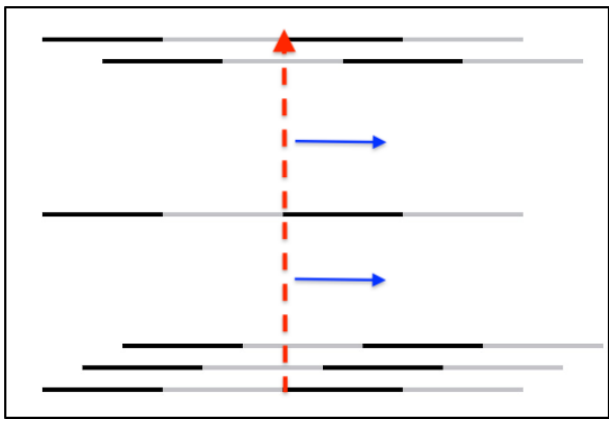

Figure 14: A sketch showing the projected incoming LLP track in red dotted line hitting the edge of a strip in the middle layer in the offset arrangement. The blue arrows show the shift of the incoming LLP.

Starting by shifting the incoming beam so that it hits at the centre of a strip in the mid-layer i.e shifting by 1/2 the strip pitch p. The distribution of the 3D displacement d_R can be produced by running the reconstruction for the first 3000 samples. This is then compared with the 0-shift condition, as shown in Figure 15.

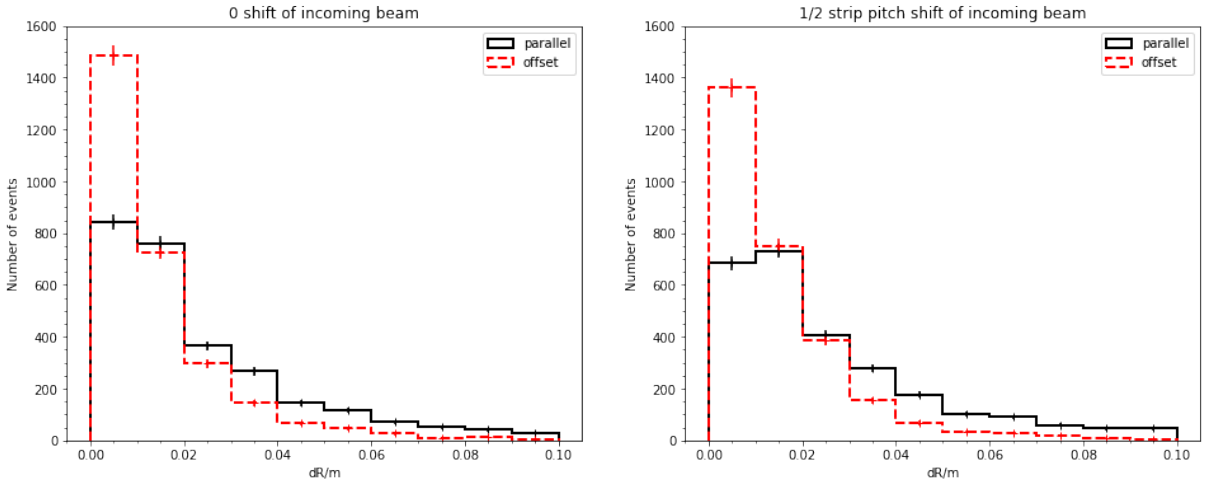

Figure 15: Distribution of dR for projected incoming LLP hitting the edge of a strip in middle-layer (left) and hitting the middle of the strip in middle-layer (right). Vertices are reconstructed using CTR method. $p = 2.5$cm, $L = 1$m.

In both cases, the distribution for the offset arrangement has a higher peak in the bin $d_R < 0.01$m, meaning the reconstructed vertex is closer to the true value. The shifted case has slightly lower peaks than the zero-shifted case for both parallel and off-set arrangements. In order to examine the full behaviour of shifting the incoming LLP, another quantitative analysis was performed. Firstly we define the percentage

of which the off-set reconstruction is better as W:

$$W_{\text{offset}} = \frac{\text{Number of events where the off-set arrangement is better}}{\text{Total number of events}} \tag{16}$$

This analysis has excluded extreme values in which reconstruction doesn't work, for instance, this could be a situation where all reconstructed tracks are near-parallel. W is plotted against the incoming LLP shift distance relative to one particular strip in the middle layer to see whether this offset arrangement is better. This graph is shown in Figure 16.

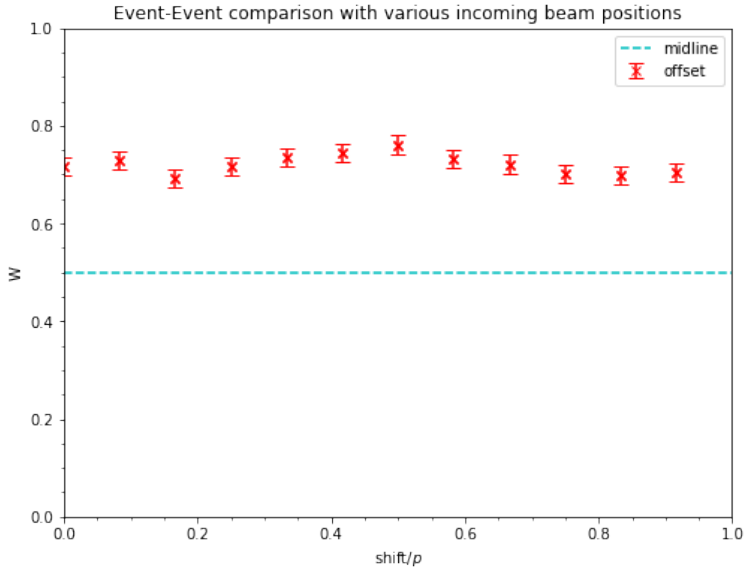

Figure 16: A event-event comparison of the two RPC layer arrangements for each event, $W = 0.5$ is the reference line and is indicated in blue, the x-axis is measured in units of strip pitch p.

For $W > 0.5$, the offset arrangement has more events that have a reconstructed vertex closer to the true vertex position. Figure 16 shows a distribution that can be approximated by a line with equation $W = 0.7$. Hence this offset arrangement is better than the parallel arrangement regardless of the projected hit position of the incoming LLP. However, the slight dips at around shift= $0.2p$ and shift= $0.8p$ show that this is not a perfect uniform distribution, but with some fluctuations embedded. The possible causes of this fluctuation are discussed in Appendix A. Therefore, for studies in sections 5.3 and 5.4, a random shift position will be selected to smear out this fluctuation error.

5.2 Repeated hits on Same strip

Before moving to see the effect of varying the distance between RPC detectors and the decay point, it is important to raise the point that there is a possibility of getting more than one hit on the same strip in one event. In this case, the detector loses the ability to identify correctly how many tracks went through, therefore the tracks would not be resolved when information about hit points is lost. Although in this study, the assumption is made that we have prior knowledge of which track hits to connect, hence it will not be affected by having repeated hits, it would be better to choose the region where the effect is minimised so that this study can be compromised to a case which is closer to reality. Figure 17 is produced to illustrate how the number of repeated hits (N_R) is affected by varying RPC distance. Note

that the distance here is the perpendicular distance from the first RPC layer to the vertex (L). As discussed in section 3.3, each RPC layer consists of x and z direction strips to give a 2D reading together, hence the repeated hits on x-strips and z-strips were analysed separately.

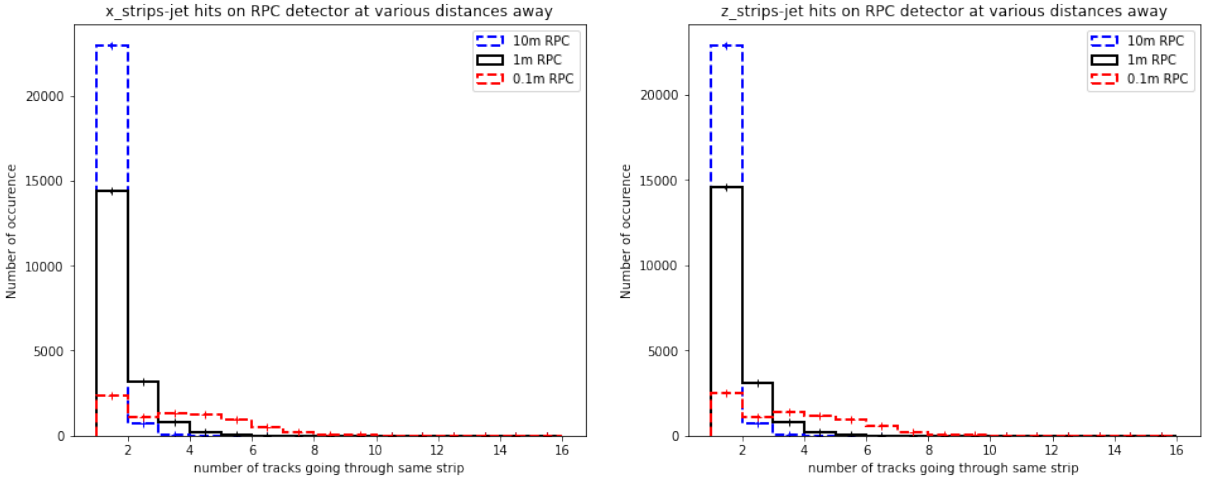

Figure 17: A histogram showing the frequency of getting repeated hits on x-strips (Left) and z-strips (Right). The first RPC layer is placed at a perpendicular distance of 0.1m (Red), 1m (Black) and 10m (Blue) away from the true decay point of LLP. Strip Pitch = 2.5 cm

Identical distributions are shown for x-strips and z-strips, this is expected due to the symmetries embedded in the final state angular distribution. RPC layer further away tends to have a higher peak at $N_R = 1$. This is because for identical particle angular distributions, the further away from the decay vertex, the more separated the tracks, hence the greater the frequency of getting $N_R = 1$. For a rough approximation, it appears that the distribution will have a clear peak at $N_R = 1$ when $L > 1$m. Hence the distance range tested in section 5.3 will be chosen to be $1 - 10$m.

5.3 RPC distance variation

Running the reconstruction process using the CTR method for the first 3000 events with RPC layers placed at different distances L (1m$< L <$ 10m) and strip pitch $p = 2.5$cm. A distribution of d_R can be plotted for each distance to see the effect of varying L. Figure 18 shows the distributions of having the first RPC layer sitting at $y =$1m, 5m and 10m.

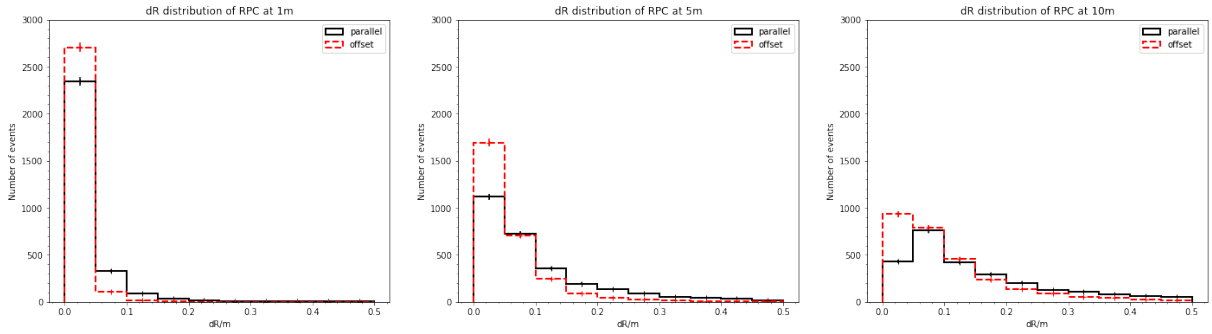

Figure 18: Distribution of dR for first RPC layer placed at 1m(left), 5m(middle) and 10m(right) away from the true vertex. The direction of incoming LLP is randomised as discussed in Section 5.1. Strip pitch fixed at $p = 2.5$cm

Figure 18 demonstrates that closer RPCs will give a better vertex reconstruction. For example, the number of events having $d_R < 0.05$m for the off-set arrangement is ~ 2700 at $L = 1$m ~ 1700 at $L = 5$m and ~ 900 at $L = 10$m. This is because the height of a single RPC tracking station H_{RPC} is 1m, and the larger the relative percentage of space covered by RPCs, the better the reconstruction will be. Hence the one which has the highest L/H_{RPC} value will give a reconstructed vertex closest to the true value.

On the other hand, in all three cases shown, the offset arrangement is either peaking at a lower value of dR or has a higher peak at the bin with the smallest dR value. This means the offset arrangement is generally better than the parallel arrangement in the range 1m$< L <$ 10m. To test this further, another event-event comparison has been performed for $L \in \{1, 2, 3, ..., 8, 9, 10\}$ (Figure 19). A near-horizontal

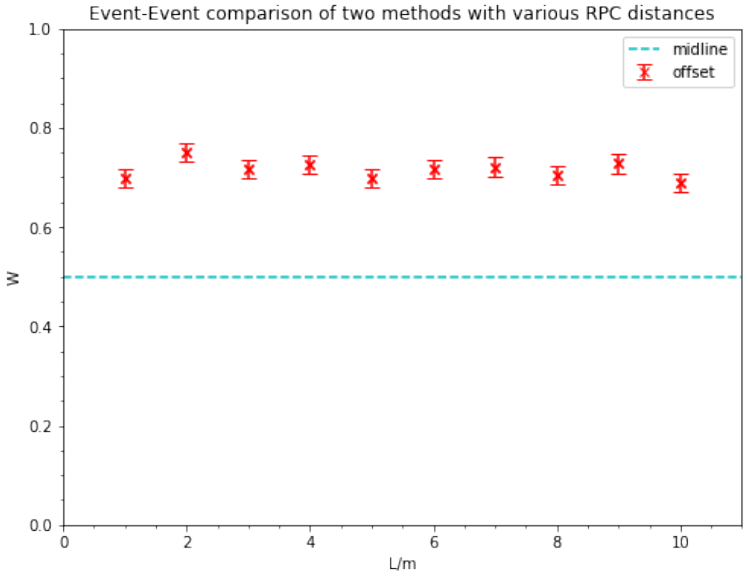

Figure 19: A direct comparison of the two RPC layer arrangements for each event, $W = 0.5$ is the reference line and is indicated in blue, this is plotted with strip pitch = 2.5cm

distribution of the points in Figure 19 at $W = 0.7$ demonstrates that $\sim 70\%$ of the events will have a

more accurate reconstructed vertex using off-set arrangement than parallel arrangement, regardless of the RPC distance L.

5.4 RPC Strip pitch variation

Similar investigations can be carried out by fixing $L = 1$m and vary the strip pitch p. Examples of the dR distributions can be found in Figure 20, where $p = 1.5$, 2.5 and $3.5cm$ are implemented suing the constrained reconstruction method with $L = 1$m. From the three examples shown, the smaller the strip

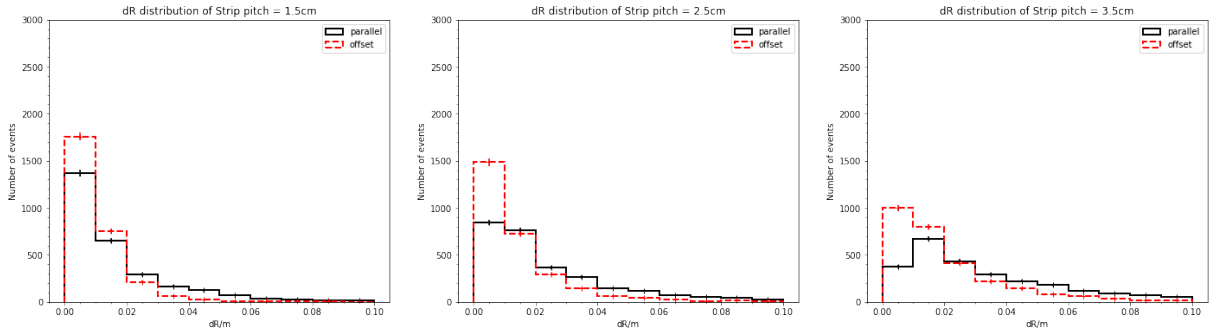

Figure 20: The distribution of dR when strip pitch is 1.5cm (Left), 2.5cm (middle) and 3.5cm (Right), with $L = 1$m. The direction of incoming LLP is randomised as discussed in Section 5.1.

pitches the higher the number of events situating at $d_R < 0.01$m i.e. the better the reconstructed vertex. This is expected as having a smaller strip increases the resolution and hence the points are more localised to their true position. It can also be demonstrated in Figure 20 that the offset arrangement is either peaking at a lower value of dR or has a higher peak at the bin with the smallest dR value. To see whether this off-set arrangement is better for all strip pitches, another event-event comparison has been carried out as shown in Figure 21. Unlike the previous event-event comparison graphs, points plotted no longer lie on a horizontal line. There is a clear positive correlation between the two variables i.e. larger the p values give larger W. The possibility of fitting a straight line through the points can be eliminated by the fact that W does not go below 0.5 at $p < 1.0$cm. This is deducted from the boundary condition that $W \to 0.5$ at $p \to 0$, as both arrangements, will just behave as point-like detectors with infinite resolution when detector sizes are infinitesimal. The information from Figure 21 can be summarised as follows: for 1.0cm$< p <$ 3.5cm, the off-set arrangement is always giving a better vertex reconstruction as all points lie above the $W = 0.5$ line; Inside this range, the advantage of using off-set arrangement is smaller with smaller detector pitches.

6 Conclusion

Beyond Standard Model theories are introduced to explain phenomena that can't be explained by the Standard Model, and many of those predict LLPs. The proposed detector ANUBIS is expected to enhance the sensitivity of LLP detection in the neutral Higgs Portal model by more than two orders of magnitude at a decay length of 10-100 m compared with the existing ATLAS analysis. This project has used Monte Carlo samples generated from the ggF channel to examine the sensitivity of vertex reconstruction in one ANUBIS tracking station with two different RPC readout strip geometries.

Two possible track and vertex reconstruction methods were introduced, the first method (ITR) fits

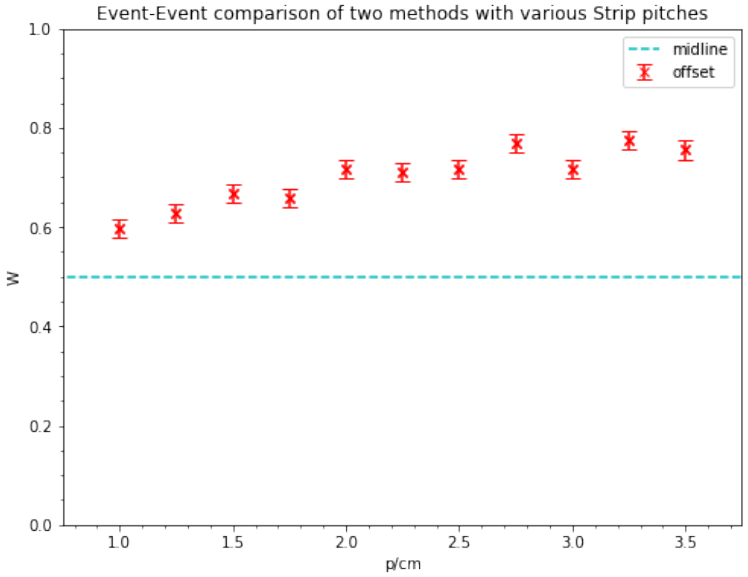

Figure 21: A direct comparison of the two RPC layer arrangements for each event, $W = 0.5$ is the reference line and is indicated in blue, this is plotted with $L = 1$m and p is varied in range 1.0cm$< p <$ 3.5cm.

each track in an event separately and then fits the vertex using reconstructed tracks; the second method (CTR) fits all tracks in one event at once with the constraint that they converge to a vertex. The distribution of the difference between reconstructed vertex position and true vertex position is plotted for each method using RPC Strip pitch $p = 2.5$cm and distance to first RPC layer $L = 1m$. The first method has a distribution peaking at $d_R \sim 0.02 - 0.03$m whereas the second method has a distribution peaking at $d_R \sim 0.00 - 0.01$m. Given the assumptions made for each method and the distributions of d_R, it is suggested to use first method 1 to identify whether tracks originate from one point, and then those selected tracks will be reconstructed again using the second method to make a more accurate vertex estimation.

In this study, two possible RPC readout strip arrangements were simulated: Parallel arranged and off-set arranged strips. Vertices were reconstructed using the CTR method and three variables were changed to see whether off-set arranged strips are generally giving a better vertex approximation environment or not. The direction of incoming LLP relative to the strips in the middle RPC layer was varied while fixing $p = 2.5$cm, $L = 1$m. The event-event comparison gives an almost horizontal distribution at $W = 0.70 \pm 0.03$, representing that this offset arrangement is better than the parallel arrangement regardless of the position of incoming LLP relative to the strips. There were small fluctuations in different directions, therefore in order to minimise this small fluctuation, a random direction was chosen for the other two analyses.

Similar investigations were performed by varying L in the range $1 - 10$m while fixing $p = 2.5cm$. Results demonstrate that closer RPCs will give a better vertex reconstruction. For instance, the number of events having $d_R < 0.05$m for the off-set arrangement is around 2700 for $L = 1$m, around 1700 for $L = 5$m. A near-horizontal distribution of the points in the event-event comparison graph at W = 0.7 demonstrates that ∼70% of the events will have a more accurate reconstructed vertex using offset arrangement than parallel arrangement, regardless of the RPC distance L. However, when the decay position is closer to the RPC the probability of getting multiple hits on the same strip increases, which reduces the resolution.

Lastly, strip pitch was varied while fixing the RPC distances. The range 1.0cm$< p <$ 3.5cm was used to cover the range of typical strip pitch (2-3cm), and L has been fixed at $1m$. Results show that smaller strip pitches tend to give a more accurate reconstructed vertex position. For example, $\sim$ 1800 events have $d_R < 0.01m$ when strips are 1.5cm wide, whereas $\sim$ 1500 events have $d_R <$ 0.01m when strips are 2.5cm wide. The event-event comparison graph illustrates that for 1.0cm$< p <$ 3.5cm, the off-set arrangement is always giving a better vertex reconstruction as all points lie above the $W = 0.5$ line; Inside this range, the advantage of using the off-set arrangement decreases when detector pitch decreases.

To conclude, although having smaller strips would increase the sensitivity, increasing the number of readout channels would also increase the cost significantly. In order to keep a balance between detector sensitivity and the cost, the strip pitch used at ATLAS and Pro-ANUBIS was chosen to be at around 2-3 cm. On the other hand, the offset arranged RPC detector is generally better than the parallel arranged case, and this condition holds with various incoming LLP positions relative to strips, RPC distances and strip pitches. This change of geometry increases the sensitivity without altering the strip pitch, and hence by implementing this configuration, the resolution of the LLP decay position can be improved with a relatively small increase in cost. By optimising the vertex resolution in Pro-ANUBIS, it is possible to test it with real data and hence can be implemented to ANUBIS.

Acknowledgement

I would like to express my deepest appreciation to Prof Oleg Brandt and Jon Burr for their support and guidance throughout this project. I also wish to thank Toby Satterthwaite for his generous help with the simulations.

Appendix A Lined-up Centre (LC) Arrangement

The fluctuations embedded in Figure 16 can be studied by first considering another geometry where the averaged centres of the triplet, singlet and the doublet layers are aligned. Figure 22 illustrates the difference between the offset arranged strips and the LC arranged strips. By performing similar analysis as before but this time using the LC arrangement, a distribution of d_R, d_{xz} and d_y can be obtained (Figure 23).

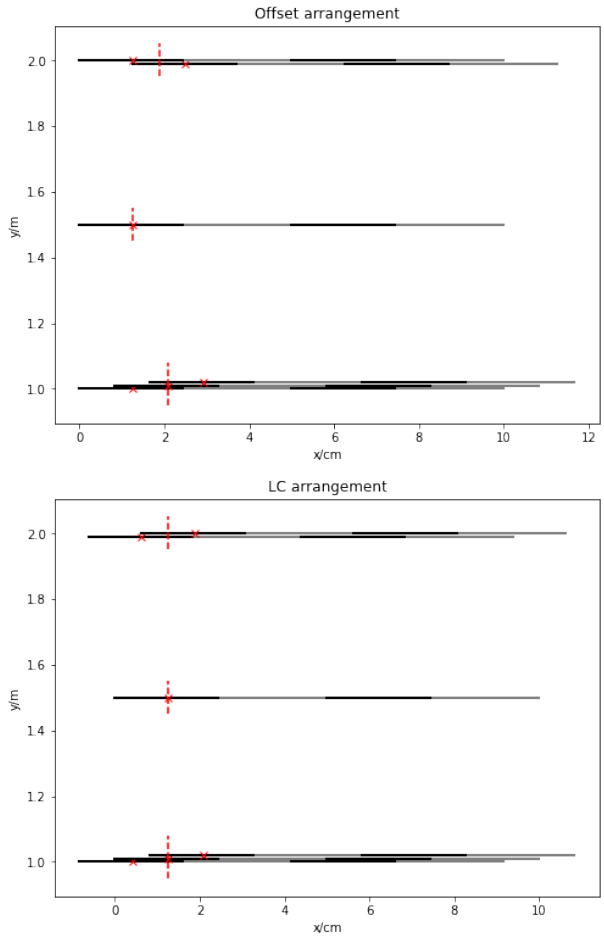

Figure 22: Diagram showing the offset arranged (Top) and lc arranged strips (Bottom). The strip centres of the first strip in each layer are labelled as red crosses, the averaged centre lines of triplet, singlet and doublets are shown as red dashed lines.

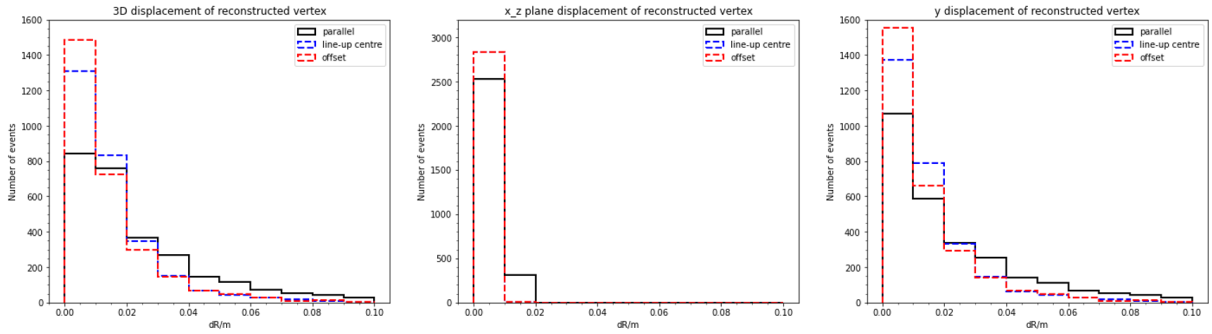

Figure 23: Distribution of the d_R (left), d_{xz} (middle) and d_y (right) using the parallel (black), offset (red) and LC (blue) arranged strips with the CTR method. L = 1m, p = 2.5cm , incoming LLP shift = 0.

Figure 23 is produced from a simulation in which the projected LLP track is hitting at exactly the edge of a strip in the middle singlet layer i.e. shift = 0. The LC arrangement has a lower peak than the normal offset arrangement but a higher peak than the parallel arrangement in the bin with the smallest value. This difference is purely caused by shifting the averaged strip centres. To study this in more detail, another event-event comparison has been performed for the first 3000 events, as demonstrated in Figure 24. In this graph, the blue points appear to have a larger fluctuation than the red points. The data points from LC arrangement appear to peak at shift$\sim 0.4 - 0.6p$ and have a minimum at shift$\sim 0.0p$ or $\sim 1.0p$. Hence, a possible explanation of the fluctuations is that a TS tends to resolve vertices better when the track is going through exactly at the averaged centres of closely packed layers. The closer the hit point is to the averaged centres of RPC layers, the better the resolution. Experimentally, it is preferred to have a flat distribution to make sure the performance is stable. Therefore a further optimisation could be done to have the averaged strip centres separated at $p/3$ to minimise this fluctuation effect.

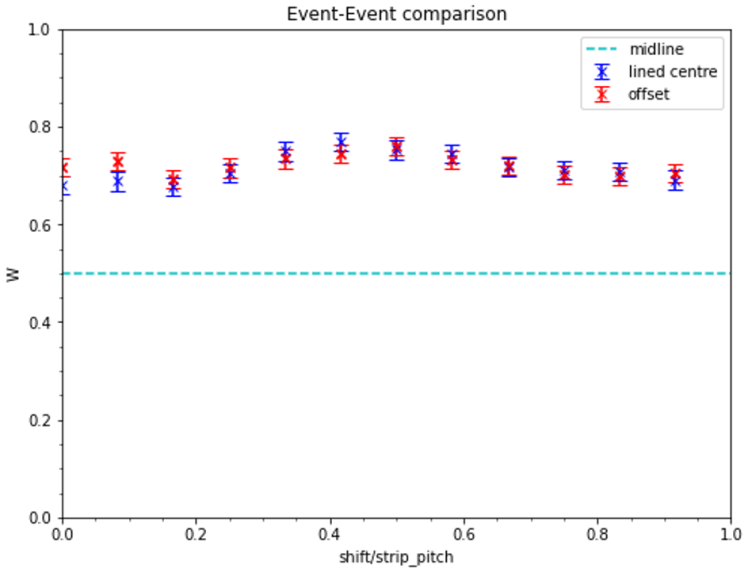

Figure 24: A event-event comparison of the RPC layer arrangements for each event, $W = 0.5$ is the reference line and is indicated in blue, the x-axis is measured in units of strip pitch p.

Appendix B ProANUBIS Simulation

Instead of rotating the incoming LLP to the direction in which it is hitting the RPC plane perpendicularly, the location of 2022 ProANUBIS is used. The LLP is rotated to simulate the detection of LLPs at the ProANUBIS: the incoming LLP now makes an angle of 10 degrees with the y-axis in the z-y plane, this matches with the prototype shown in Figure 25. An example of a typical track rotation in one event can be seen in Figure 26.

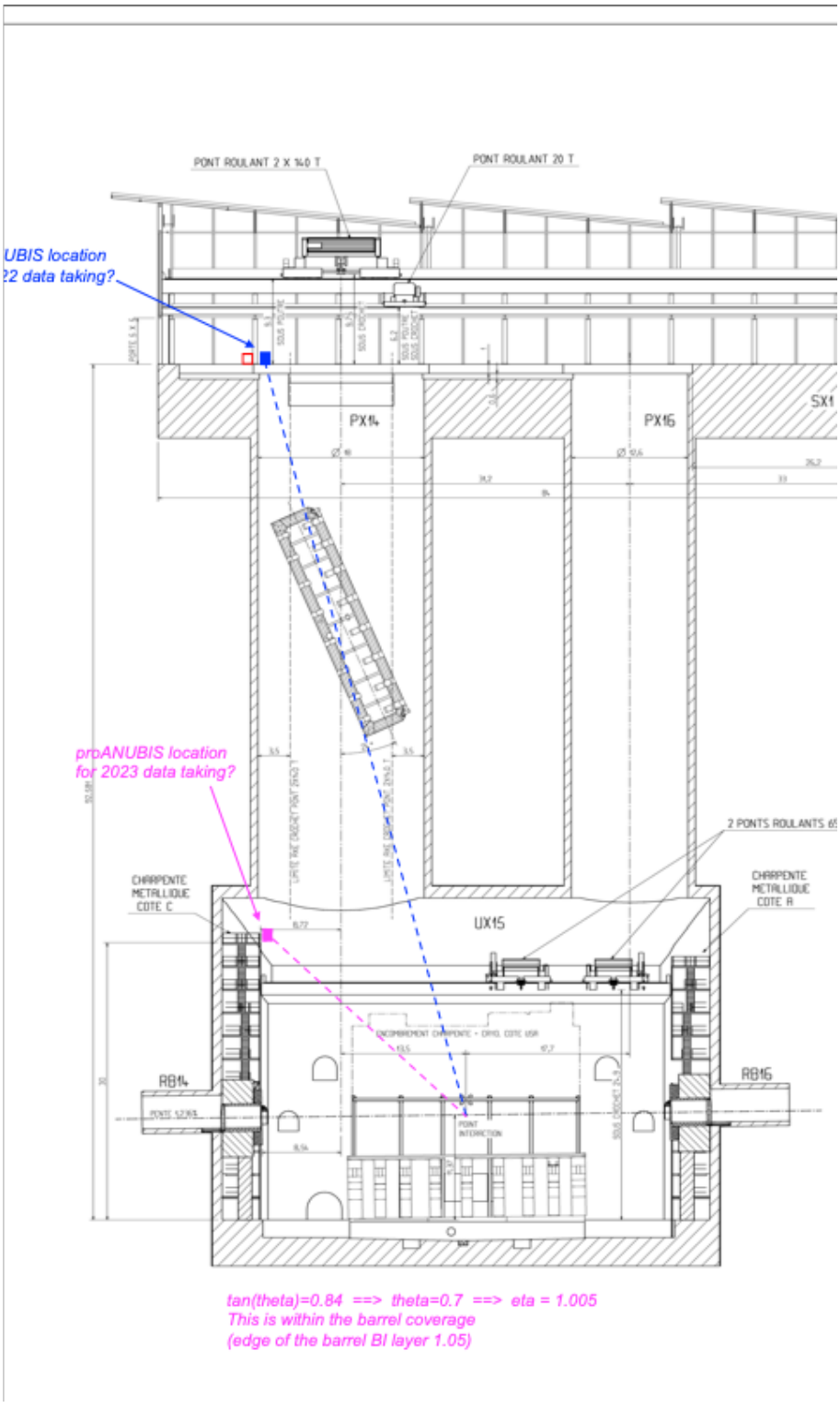

Figure 25: A side view of ATLAS cavern and shaft (in the z-y plane), the location of 2022 ProANUBIS is shown as a blue square sitting at the top of the PX14 shaft. Graph is taken from the ANUBIS group

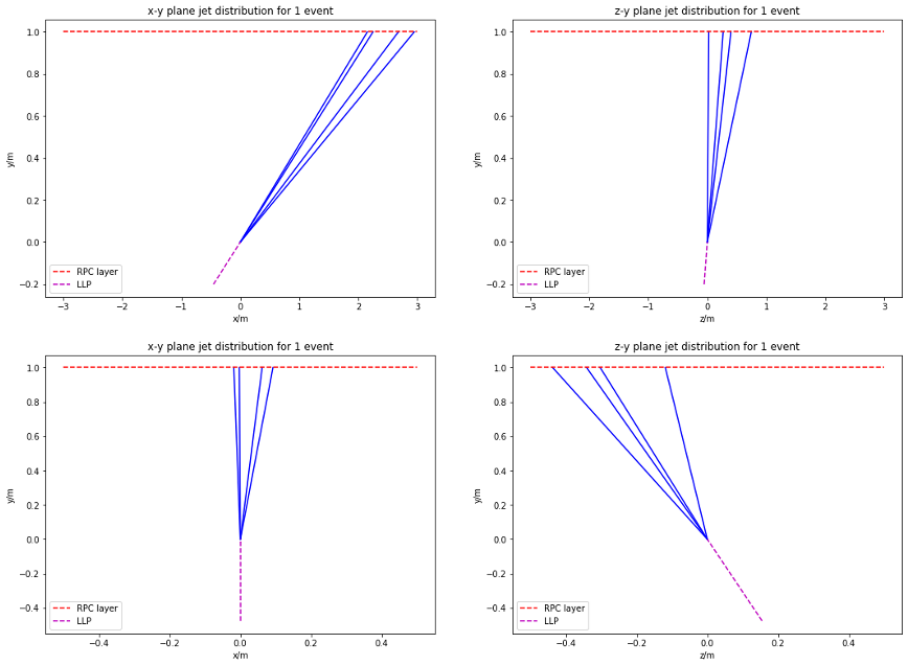

Figure 26: Top diagrams showing a typical event in x-y (left) plane and z-y (right) plane. Bottom diagrams showing the same event after rotated using 2022 ProANUBIS angular coordinates in x-y (left) plane and z-y (right) plane.

The d_R distribution can be obtained using this incoming LLP direction together with the CTR method, this is illustrated in Figure 27. The graph shows that both the lined-up centre arrangement and the offset arrangement have a higher peak at the bin with the smallest value, hence the argument that offset arranged strips improve sensitivity still applies even when LLPs are not coming in perpendicular to the RPC plane.

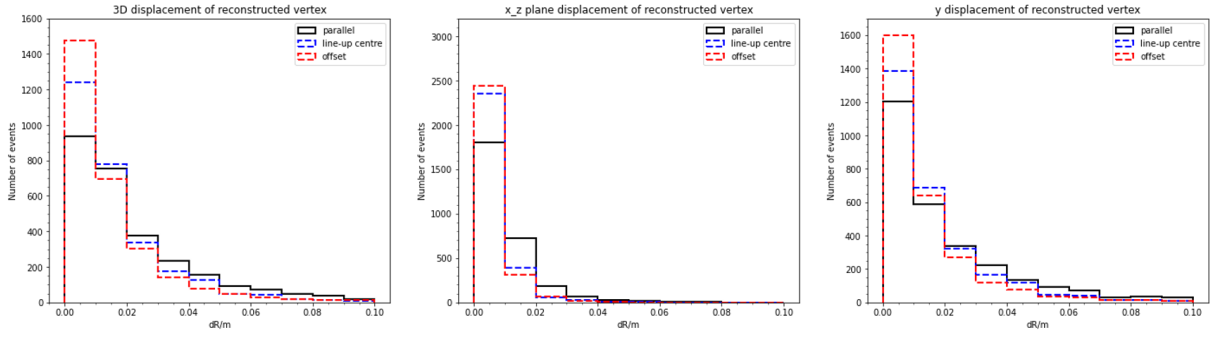

Figure 27: A simulation using the ProANUBIS directed LLPs decaying at L=1m, and strip pitch p=2.5cm.

Appendix C Detector Simulation Code Examples

C.1 Track Rotation

```
def to_theta(eta):
    return 2 * np.arctan(np.exp(-eta))

# Convert to cartesian
def to_cartesian(r, theta, phi):
    x = r * np.sin(theta) * np.cos(phi)
    y = r * np.sin(theta) * np.sin(phi)
    z = r * np.cos(theta)

    return x, y, z

def rotation(phi,theta,x,y,z):
    #first rotation w.r.t. z axis by angle pi/2-phi counter
       clockwise
    #Transform particle to the z-y plane
    phi_rot = np.pi/2 - phi
    x_1 = np.multiply(np.cos(phi_rot),x) - np.multiply(np.sin(
       phi_rot),y)
    y_1 = np.multiply(np.sin(phi_rot),x) + np.multiply(np.cos(
       phi_rot),y)
    z_1 = z

    #second rotation w.r.t x axis by angle pi/2-theta clockwise-
       reverse
    #Transform beam to the y-axis
    theta_rot = np.pi/2 - theta
    x_2 = x_1
    y_2 = np.multiply(np.cos(theta_rot),y_1) + np.multiply(np.sin(
       theta_rot),z_1)
    z_2 = -np.multiply(np.sin(theta_rot),y_1) + np.multiply(np.cos
       (theta_rot),z_1)
    return x_2, y_2, z_2
```

C.2 Track hit simulation

```
def intersect(x_m, y_m, z_m, RPC_height):
    x = np.divide(x_m, y_m)*RPC_height
    z = np.divide(z_m, y_m)*RPC_height
    y = [RPC_height]*len(x)
    x = list(x)
    z = list(z)
```

```
    return x,y,z

def multiple_hit(strip_width, x, z, n, m): # nth position of a
    shift of 1/m * strip width
    strip_x=[]
    strip_z=[]
    for i in range(len(x)):
        #floor returns the lowest integer value
        round_x = math.floor((x[i]-strip_width*(n/m))/strip_width)
            *strip_width
        round_x = round_x + strip_width/2 + strip_width*(n/m)
        strip_x.append(round_x)
        round_z = math.floor((z[i]-strip_width*(n/m))/strip_width)
            *strip_width
        round_z = round_z + strip_width/2 + strip_width*(n/m)
        strip_z.append(round_z)
    return strip_x, strip_z
```

The first function is used to find the points at which true tracks intersects the RPC layers. The second function is used to approximate this actual hit point to strip read point.

C.3 CTR method

To calculate the χ^2 term:

```
def get_mse(params, x, y, z):
    rx, ry, rz = params[:3]
    gradients = params[3:]
    sigma = 0.025/np.sqrt(12)
    mx = np.reshape(gradients[::2], (-1,1))
    mz = np.reshape(gradients[1::2], (-1,1))
    mse_z = np.mean(np.square((z - mz*(y-ry)-rz)/sigma))
    mse_x = np.mean(np.square((x - mx*(y-ry)-rx)/sigma))
    return mse_x + mse_z
```

Then input this into the optimising function to minimise χ^2:

```
opt = optimize.minimize(get_mse, param0, args = (x_set, y_set,
    z_set), options = {'maxiter': 1000} )
#param0 is a vector consisting of the vertex position, the x-y and
    z-y gradients
```

References

[1] Technical Design Report for the Phase-II Upgrade of the ATLAS TDAQ System. Sep 2017. doi: 10.17181/CERN.2LBB.4IAL. URL https://cds.cern.ch/record/2285584.

[2] Technical Design Report for the Phase-II Upgrade of the ATLAS Muon Spectrometer. Sep 2017. URL https://cds.cern.ch/record/2285580.

[3] Search for Higgs boson decays into long-lived particles in associated Z boson production. 2021. URL https://cds.cern.ch/record/2767507.

[4] M. Aaboud, G. Aad, B. Abbott, O. Abdinov, B. Abeloos, D. Abhayasinghe, S. Abidi, O. AbouZeid, and e. a. N. L. Abraham. Search for long-lived particles produced in pp collisions at s=$\sqrt{13}$ tev that decay into displaced hadronic jets in the atlas muon spectrometer. *Physical Review D*, 99(5), mar 2019. doi: 10.1103/physrevd.99.052005. URL https://doi.org/10.1103%2Fphysrevd.99.052005.

[5] M. Aaboud et al. Search for long-lived neutral particles in pp collisions at $\sqrt{s} = 13$ TeV that decay into displaced hadronic jets in the ATLAS calorimeter. *Eur. Phys. J. C*, 79(6):481, 2019. doi: 10.1140/epjc/s10052-019-6962-6.

[6] G. Aad et al. Search for exotic decays of the Higgs boson into long-lived particles in pp collisions at $\sqrt{s} = 13$ TeV using displaced vertices in the ATLAS inner detector. *JHEP*, 11:229, 2021. doi: 10.1007/JHEP11(2021)229.

[7] R. Aaij, , B. Adeva, M. Adinolfi, Z. Ajaltouni, S. Akar, J. Albrecht, F. Alessio, M. Alexander, S. Ali, G. Alkhazov, P. A. Cartelle, A. A. Alves, and et al. Updated search for long-lived particles decaying to jet pairs. *The European Physical Journal C*, 77(12), nov 2017. doi: 10.1140/epjc/s10052-017-5178-x. URL https://doi.org/10.1140%2Fepjc%2Fs10052-017-5178-x.

[8] J. Alwall, R. Frederix, S. Frixione, V. Hirschi, F. Maltoni, O. Mattelaer, H.-S. Shao, T. Stelzer, P. Torrielli, and M. Zaro. The automated computation of tree-level and next-to-leading order differential cross sections, and their matching to parton shower simulations. *Journal of High Energy Physics*, 2014(7), jul 2014. doi: 10.1007/jhep07(2014)079. URL https://doi.org/10.1007%2Fjhep07%282014%29079.

[9] A. Ariga, T. Ariga, J. Boyd, F. Cadoux, D. W. Casper, Y. Favre, and J. L. F. et al. FASER's physics reach for long-lived particles. *Physical Review D*, 99(9), may 2019. doi: 10.1103/physrevd.99.095011. URL https://doi.org/10.1103%2Fphysrevd.99.095011.

[10] M. Bauer, O. Brandt, L. Lee, and C. Ohm. Anubis: Proposal to search for long-lived neutral particles in cern service shafts, 2019.

[11] R. Cardarelli, G. Aielli, E. A. Camelia, S. Bruno, A. Caltabiano, P. Camarri, A. D. Ciaccio, B. Liberti, L. Massa, L. Pizzimento, and et al. Rpc performance versus front-end electronics and detector parameters. *Journal of Instrumentation*, 14(09):C09023–C09023, Sep 2019. ISSN 1748-0221. doi: 10.1088/1748-0221/14/09/c09023. URL http://dx.doi.org/10.1088/1748-0221/14/09/C09023.

[12] D. Curtin, M. Drewes, M. McCullough, P. Meade, R. N. Mohapatra, J. Shelton, B. Shuve, and et al. Long-lived particles at the energy frontier: the MATHUSLA physics case. *Reports on Progress in Physics*, 82(11):116201, oct 2019. doi: 10.1088/1361-6633/ab28d6. URL https://doi.org/10.1088%2F1361-6633%2Fab28d6.

[13] J. L. Feng, I. Galon, F. Kling, and S. Trojanowski. ForwArd search ExpeRiment at the LHC. *Physical Review D*, 97(3), feb 2018. doi: 10.1103/physrevd.97.035001. URL https://doi.org/10.1103%2Fphysrevd.97.035001.

[14] V. V. Gligorov, S. Knapen, M. Papucci, and D. J. Robinson. Searching for long-lived particles: A compact detector for exotics at LHCb. *Physical Review D*, 97(1), jan 2018. doi: 10.1103/physrevd.97.015023. URL https://doi.org/10.1103%2Fphysrevd.97.015023.

[15] L. Lee, C. Ohm, A. Soffer, and T.-T. Yu. Collider searches for long-lived particles beyond the standard model. *Progress in Particle and Nuclear Physics*, 106:210–255, May 2019. ISSN 0146-6410. doi: 10.1016/j.ppnp.2019.02.006. URL http://dx.doi.org/10.1016/j.ppnp.2019.02.006.

[16] H. Lubatti, C. Alpigiani, J. C. Arteaga-Velázquez, A. Ball, and e. a. Beacham. Mathusla: A detector proposal to explore the lifetime frontier at the hl-lhc, 2019. URL https://arxiv.org/abs/1901.04040.

[17] L. Pizzimento. Performance of the bis78 rpc detectors: a new concept of electronics and detector integration for high-rate and fast timing large size rpcs. *Journal of Instrumentation*, 15 (11):C11010–C11010, Nov 2020. ISSN 1748-0221. doi: 10.1088/1748-0221/15/11/c11010. URL http://dx.doi.org/10.1088/1748-0221/15/11/C11010.

[18] A. M. Sirunyan, A. Tumasyan, W. Adam, F. Ambrogi, T. Bergauer, M. Dragicevic, J. Erö, and e. a. Escalante Del Valle. Search for long-lived particles using displaced jets in proton-proton collisions at $\sqrt{s} = 13$ TeV. *Phys. Rev. D*, 104:012015, Jul 2021. doi: 10.1103/PhysRevD.104.012015. URL https://link.aps.org/doi/10.1103/PhysRevD.104.012015.

[19] P. Virtanen, R. Gommers, T. E. Oliphant, and et al. Scipy 1.0: Fundamental algorithms for scientific computing in python. *Nature Methods*, 17:261–272, 2020. doi: 10.1038/s41592-019-0686-2. URL https://rdcu.be/b08Wh.